Journal of Applied Polymer Science

The effect of ceria nanoparticles on improving heat resistant properties of fluorosilicone rubber

Xiang Xu,[1] Junjie Liu,[1] Pei Chen,[1] Dafu Wei,[1] Yong Guan,[1] Xiaojuan Lu,[2] Huining Xiao[2]

[1]Key Laboratory for Ultrafine Materials of Ministry of Education, School of Materials Science and Engineering, East China University of Science and Technology, Shanghai 200237, China

[2]School of Environmental Science and Engineering, North China Electric Power University, Baoding 071000, China

Correspondence to: Y. Guan (E-mail: yguan@ecust.edu.cn) and H. Xiao (E-mail: hnxiao@ncepu.edu.cn)

ABSTRACT: The thermal aging behavior of poly(3,3,3-trifluoropropyl)methylsiloxane was investigated by thermal gravimetric analysis and isothermal aging tests, and the results indicated the degradation mechanism II, oxidation scission of the side groups, played a more important role when the temperature was below 350 °C. The addition of ceria had significantly improved the thermal stability of fluorosilicone rubber (FSR) by inhibiting the oxidation scission. Moreover, two types of ceria including laminar-structure ceria (LS-CeO_2) and nanoparticle ceria (N-CeO_2) were prepared and surface was modified by KH570 and characterized by scanning electron microscopy, transmission electron microscope, and X-ray diffractometer. FSR incorporated with modified LS-CeO_2 and N-CeO_2 revealed a significant improvement on the heat resistant properties. In particular, after having been thermal oxidative aged for 70 h at 250 °C, FSR containing 2 wt % of modified N-CeO_2 maintained 72.6% of tensile strength and 63.9% of elongation at break, respectively, while FSR without ceria completely failed. © 2016 Wiley Periodicals, Inc. J. Appl. Polym. Sci. **2016**, *133*, 44117.

KEYWORDS: ageing; degradation; nanoparticles; nanowires and nanocrystals; thermal properties; rubber

Received 4 February 2016; accepted 23 June 2016

DOI: 10.1002/app.44117

INTRODUCTION

Fluorosilicone rubber (FSR), which is well known for excellent oil and fuel resistance in a wide operating temperature range (−60 to 200 °C) has found wide application in automotive and aircraft industries, petroleum-related equipments, and so on.[1–9] As one of the few elastomers used in extreme conditions, FSR needs to be modified to enhance its heat resistance, enabling to serve for new technology.[10–13] For example, in the twin turbos, the turbocharger hoses are often exposed to tail gas with temperature up to 250 °C. As is well known, the silicone rubbers (SR) tend to deteriorate at temperature above 200 °C for extended periods of time, because of two mechanisms: (1) the degradation or reversion of the main chain to generate low molecular weight cyclosiloxanes; (2) the oxidation scission of the side groups.[14,15] However, FSR is even less heat stable than SR because FSR is more susceptible to siloxane bond cleavage and oxidative degradation.[16–18]

It has been common practice to add metal oxides (Fe_2O_3, CeO_2, SnO_2, etc.) or some metallic compounds in an attempt to improve the thermal stability of silicone elastomers, by eliminating radicals generated from thermal oxidation.[19–21] Among them ceria (or cerium dioxide) is the mostly used antioxidant for FSR because of its high efficiency.[22,23] However, ceria as sold in the market (MS-CeO_2), with a low specific surface area, needs a large addition amount, thus causing the deterioration of mechanical properties of FSR.

The purpose of this study is to improve the thermal stability of FSR by adding nanoscale ceria. Two types of ceria including laminar-structure ceria (LS-CeO_2) and nanoparticle ceria (N-CeO_2) were prepared and modified by silane coupling agent. The thermal stability of FSR incorporating of MS-CeO_2, nano-scale ceria and modified nano-scale ceria were evaluated through thermal oxidative aging. In the end, the thermal degradation mechanism of FSR and the antioxidant effect of ceria were discussed.

EXPERIMENTAL

Materials

Cerium(III) nitrate hexahydrate (≥99.5%), sodium bicarbonate (≥99.5%), sodium chloride (≥99%), ethylene glycol (≥99%), and [3-(Methacryloyloxy)propyl]trimethoxysilane (KH570, ≥98%) were purchased from Sinopharm Chemical Reagent (Shanghai, China). Poly(3,3,3-trifluoropropyl) methylsiloxane (PTFPMS, $M_w = 8 \times 10^5$, $M_w/M_n = 1.5$, incorporating of 0.4 mol % of methylvinylsiloxane units) was obtained from FSIR Advanced Material (Zhenjiang, China). Hydrophobic

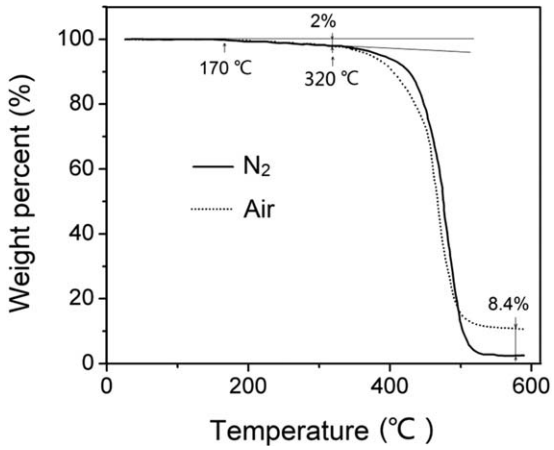

Figure 1. TGA traces of PTFPMS in nitrogen and in air.

fumed silica aerosol R812 (surface area equals to 260 ± 30 m^2/g) was purchased from Evonic Degussa. Shanghai Branch (Shanghai, China). 2, 5-Dimethyl-2, 5-di(tert-butyl) peroxyhexane (DBPMH) was obtained from Sendy Chem (Shanghai, China).

Preparation of LS-CeO_2

Cerium(III) nitrate hexahydrate (21.7 g, 0.05 mol) was dissolved in 200 mL deionized water to get solution A, and sodium bicarbonate (15.1 g, 0.18 mol) was dissolved in 200 mL deionized water to get solution B. Then solution A was slowly added to solution B with vigorous stirring, and white precipitate appeared immediately. After about 15 min of stirring, the precipitate was filtrated, washed with deionizedwater and dried in a vacuum oven at 50 °C for 4 h. The resulting precursor was calcined in a muffle furnace at 350 °C for 4 h, and light yellow powders with loose structure were obtained, namely LS-CeO_2.

Preparation of N-CeO_2

CeO_2 nanopaticles were prepared by a solution combustion synthesis (SCS) as follows.[24,25] Cerium(III) nitrate hexahydrate (21.7 g, 0.05 mol), ethylene glycol (2.3 g, 0.0375 mol), and sodium chloride (4.4 g, 0.075 mol) were dissolved in deionized water to obtain transparent solution, and then a part of water was evaporated using a oil bath at 110 °C till the solution became viscous. Then the viscous solution was placed in a crucible and calcined in a muffle furnace at 250 °C. The expansion of the solution, spontaneous combustion, and intense discharge of gas in the combustion process were observed. Finally, the loose structure powders were washed with deionized water to remove unreacted ceriumnitrate hexahydrate and sodium chloride. The final product, N-CeO_2, was obtained after being dried.

Surface Modification of CeO_2 Using KH570

Ten gram of LS-CeO_2 (or N-CeO_2), 1.5 g of KH570, and 100 mL of ethanol (90%) were charged in a 500 mL beaker equipped with a magnetic stir bar; 0.2 mL of acetic acid was used as catalyst. The mixture was stirred at room temperature overnight. The modified CeO_2 was obtained after filtration, washing with ethanol and drying, namely mLS-CeO_2 (or mN-CeO_2).

Preparation of FSR Test Specimens

The FSR compounds were prepared by blending 60 g of PTFPMS, 24 g of R812, and varied amount of CeO_2 in a torque rheometer (SU-70, Changzhou Suyan Science and Technology Corp., China) at 150 °C for 20 min. Then, 1 wt % of DBPMH was blended into each compound using a two-roll mill (760, Jiangdu Xuanyu Experimental Machinery Plant, China). The resulting compounds were charged in a $150 \times 150 \times 2$ mm^3 die for the vulcanization, which was performed using a plate vulcanization machine (BL-6170-A, Bolon Precision Testing Machines, China) at 170 °C and 10 MPa for 10 min and then post-cured in an oven at 200 °C for 4 h. The test specimens for mechanical properties were prepared according to ASTM D412.

Characterizations

FTIR spectra of aged PTFPMS were recorded on a Nicolet 5700 infrared spectrometer (Thermo Electron Scientific Instruments Corp). Each spectrum was an average of 32 spectra measured at a resolution of 2 cm^{-1} between 4000 and 400 cm^{-1}. Thermo gravimetric analysis (TGA) was performed in nitrogen or air atmosphere between 20 and 800 °C at a heating rate of 10 °C/min using a universal V4.5A TA instrument SDTQ600 V20.9

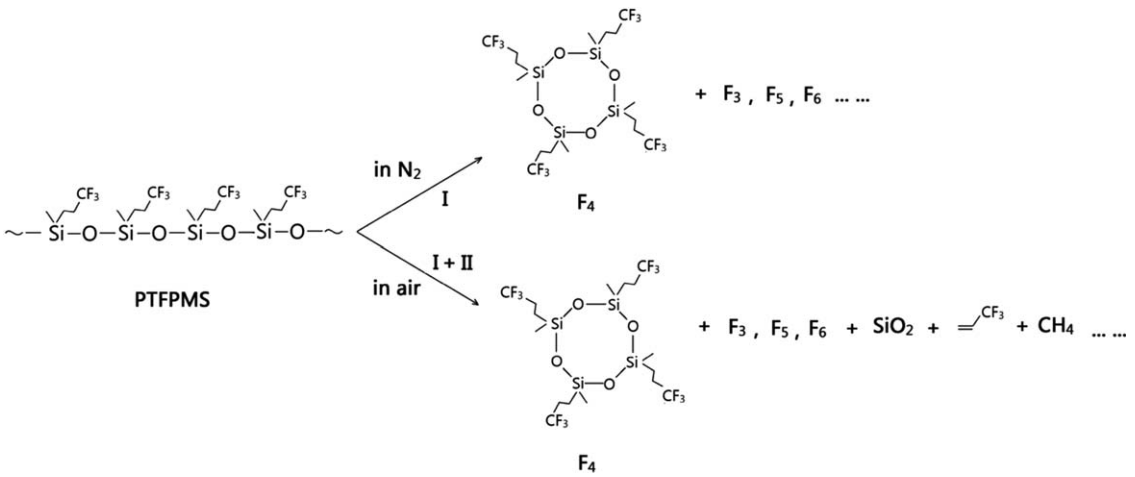

Figure 2. Thermal degradation of PTFPMS in nitrogen and in air.

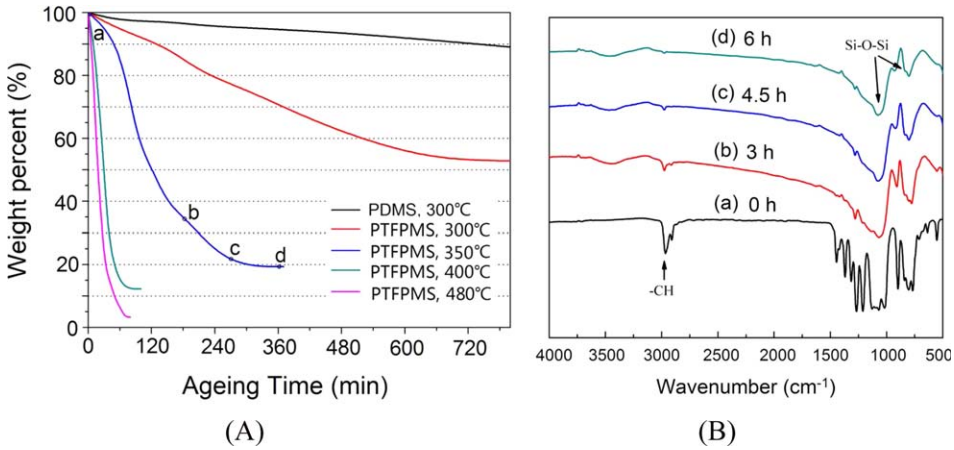

Figure 3. Isothermal weight-loss curves of PDMS and PTFPMS in air atmosphere (A) and the FTIR spectra of aged PTFPMS corresponding to isothermal weight-loss curve of PTFPMS at 350 °C (B). [Color figure can be viewed in the online issue, which is available at wileyonlinelibrary.com.]

Build 20 (TA Instruments). Scanning electron microscopy (SEM) images were taken by the JSM-6360LV (JEOL, Japan) at an accelerating voltage of 15 kV. The SEM samples were gold-sputtered prior to the observation. The transmission electron microscope (TEM) of N-CeO_2 was observed in bright-field using a JEOL 2000FX TEM (JEOL, Japan) operating at 200 kV. The crystalline structures of M-CeO_2, LS-CeO_2, mLS-CeO_2, and N-CeO_2 were investigated by using an X-ray diffractometer (XRD, D/max2200PC, Rigaku). The crystallite size of N-CeO_2, d_{XRD}, can be estimated from XRD patterns by applying full-width half-maximum (FWHM) of characteristic peak (111) to the Scherrer equation:

$$d \times \mathrm{RD} = \frac{0.89\lambda}{\mathrm{FWHM}\cos\theta} \quad (1)$$

where λ is the X-ray wavelength (0.15418 nm in this study) and θ is the diffraction angle for the (1 1 1) plane.

The isothermal aging test was carried out in a TCXC-1700 muffle furnace (Shanghai Tongcoo Electric Equipment, China). The PTFPMS or PTFPMS/silica/CeO_2 specimens were charged in graphite crucibles and placed in the muffle furnace setting to 350 °C. The mass of each specimen was recorded at an interval of 15 min. The element analysis of PTFPMS aging after 0, 3, 4.5, and 6 h were performed by a Bruker Qauntax 400 energy dispersive spectrometer (EDS).

The tensile strength (TS) and elongation at break of the FSR were measured using an electronic universal testing machine CMT-400 (Zhuhai SUST Electrical Equipment, China) according to ISO 37:2005. The type of test piece was dumb-bell type 1, and the rate of traverse was set to 500 mm/min. The thermal aging treatment was performed in an aging oven XY-401 (Jiangdu Xuanyu testing machinery factory, China).

Table I. Element Analysis of aged PTFPMS

Ageing time	Si wt %	F wt %	C wt %	O wt %
0 h	17.9	36.5	30.8	10.3
3 h	50.6	7.2	8.9	33.3
4.5 h	48.5	5.6	9.8	36.1
6 h	51.5	5.1	6.0	37.4

RESULTS AND DISCUSSION

The Thermal Aging Behavior of PTFPMS

Figure 1 shows the TGA traces of PTFPMS (the matrix polymer of FSR) in nitrogen and in air, respectively. The polymer reveals good thermal stability till 320 °C both in nitrogen and in air. The 2% of weight loss is possibly due to the residual cyclic monomers. The PTFPMS started to deteriorate from 320 °C, and revealed a faster degradation in air.

The studies on thermal degradation of PDMS[26,27] presented two mechanisms for polysiloxanes: the siloxane rearrangement to give cyclic oligmers (I) and oxidation scission of the side groups (II). Those two mechanisms are suitable for the PTFPMS. As shown in Figure 2, in nitrogen, the degradation follows mechanismI. The PTFPMS was completely deteriorated into cyclic oligmers and volatilized, leaving a slight residues.[28] However, in air, the oxidation scission happened along with the siloxane rearrangement. A part of side groups suffered from oxidation scission and became methane, trifluoropropene or other chemicals. The remaining —Si—O— chain could not rearrange,

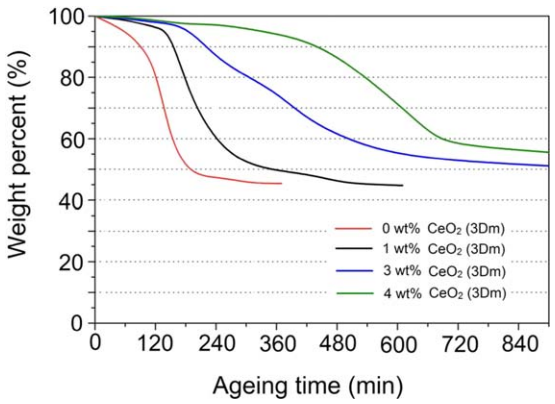

Figure 4. .Isothermal weight-loss curves of PTFPMS/silica/mN-CeO_2 in air atmosphere under 350 °C. [Color figure can be viewed in the online issue, which is available at wileyonlinelibrary.com.]

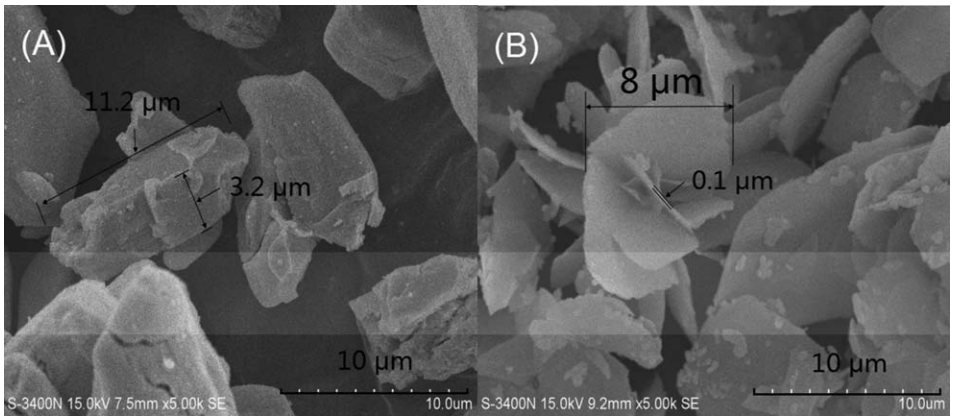

Figure 5. SEM imagesof (A) MS-CeO_2 and (B) LS-CeO_2.

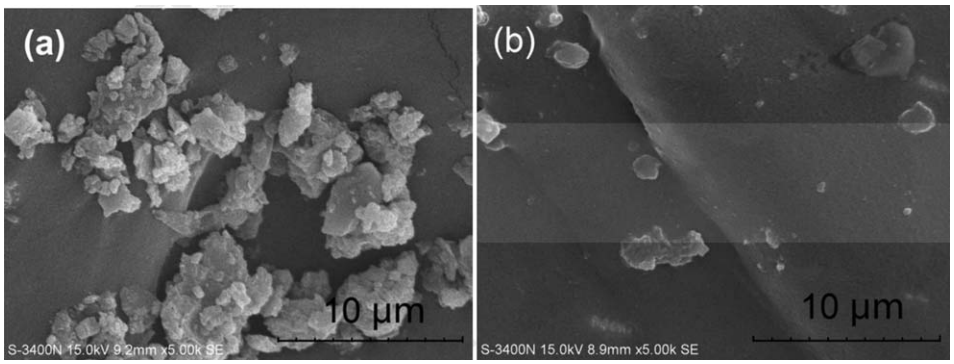

Figure 6. SEM images of fracture sections of (a) PTFPMS/silica/LS-CeO_2(100/40/2) and (b) PTFPMS/silica/mLS-CeO_2 (100/40/2).

resulting in the residue—SiO_2 . Therefore, there was an additional 8.4% of residue left when thermally degraded in air (see Figure 1).

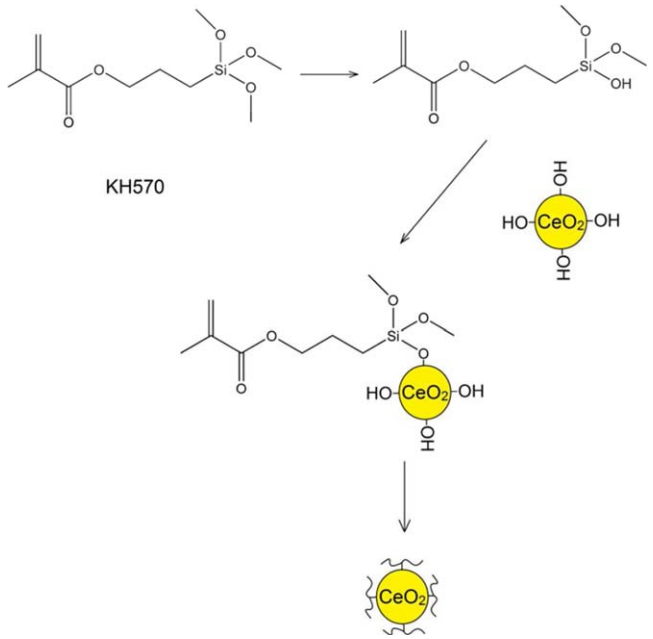

Figure 7. Surface modification mechanism of CeO_2. [Color figure can be viewed in the online issue, which is available at wileyonlinelibrary.com.]

To further evaluate the thermal aging resistance of PTFPMS, isothermal aging of PTFPMS were performed and the isothermal weight-loss curves in air atmosphere under 300, 350, 400, and 480 °C are shown in Figure 3. For the isothermal aging at 300 °C, the weight-loss curve of PDMS was also recorded for comparison. The result shows that PTFPMS deteriorated more

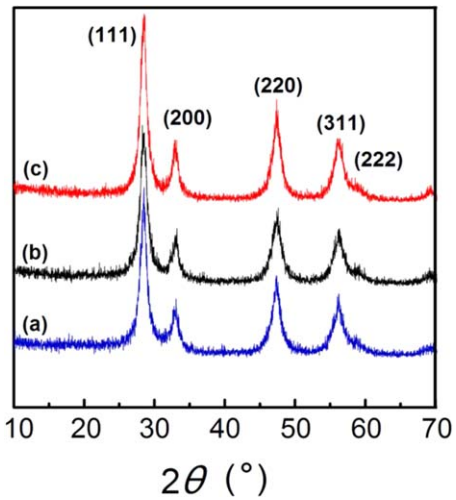

Figure 8. XRD patterns of (a) MS-CeO_2; (b) LS-CeO_2; (c) mLS-CeO_2. [Color figure can be viewed in the online issue, which is available at wileyonlinelibrary.com.]

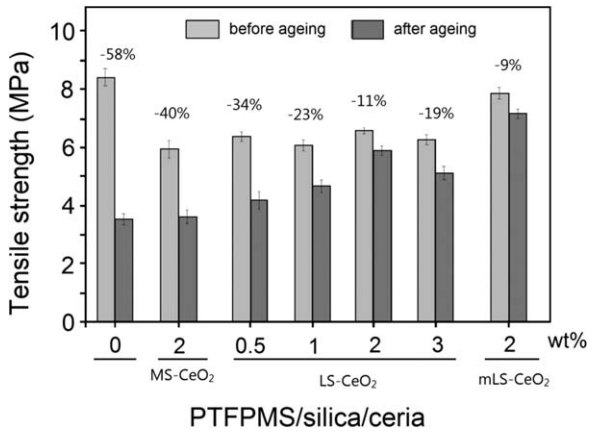

Figure 9. The TS of FSR incorporating of CeO_2 before and after aging at 230 °C for 70 h.

intensively than PDMS. It is easy to understand the PTFPMS is more susceptible to siloxane bond cleavage because of the electron withdrawing inductive effect of 3,3,3-trifluoropropyl group. Moreover, the —CH_2— was easier to be oxidized than —CH_3.

From the isothermal weight-loss curves of PTFPMS, the PTFPMS deteriorated more and more rapidly with temperature increasing from 300 to 480 °C, and the residual weight decreased from 53 to 3% correspondingly. Whether if the residual weight could represent the percentage of mechanism II? The structure of residual was identified by FTIR and EDS measurements.

The FTIR spectra [see Figure 3(B)] and element analysis (see Table I) of aged PTFPMS after 0, 3, 4.5, and 6 h were investigated. From FTIR spectra, the organic components (such as —CH_3 or —$CH_2CH_2CF_3$) decreased gradually from 0 to 6 h and finally only inorganic silicon dioxide was left. The EDS data quantitatively verified such variation. The element F and C showed a large weight loss, from 36.5 and 30.8% to 1.1% (5.6 × 20%) and 2% (9.8 × 20%), respectively, where 20% is the weight percent of residue from Figure 3(A). The weight percentage of element Si decreased from 17.9 to 10.3%, suggesting 42.5% of element Si evaporated in the form of cyclic oligmers. As a result, in the isothermal aging of PTFPMS at 350 °C, the

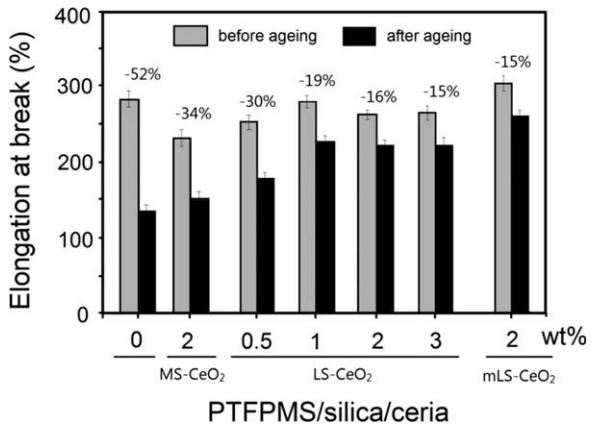

Figure 10. The elongation at break of FSR incorporating of CeO_2 before and after aging at 230 °C for 70 h.

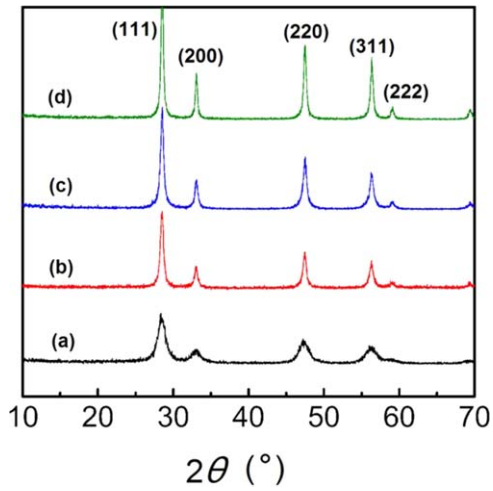

Figure 11. XRD patterns of N-CeO_2 when (a) φ = 0.75; (b) φ = 1; (c) φ = 1.5; (d) φ = 2.25. [Color figure can be viewed in the online issue, which is available at wileyonlinelibrary.com.]

percentage of degradation resulted from mechanism II, 57.5%, outweighs mechanism I. When the temperature was below 350 °C, the degradation of PTFPMS was mainly resulted from oxidation scission of the side groups.

The Antioxidant Property of Ceria

In many studies, the metal oxides were used as antioxidant for SRs.[19–21] For example, the ceria could eliminate the free radical by redox reaction from Ce^{4+} to Ce^{3+}, and the Ce^{3+} could revert to Ce^{4+} by the oxidation of oxygen.[29–31] By the oxidation- reduction recycles, the ceria could inhibit the degradation resulted from mechanism II continuously.

Figure 4 shows the isothermal aging of PTFPMS/silica/mN-CeO_2 in air atmosphere at 350 °C. Due to the separation effect of silica,[32] the compound (PTFPMS/silica) stood a longer time to reach the maximum degradation rate than PTFPMS. The

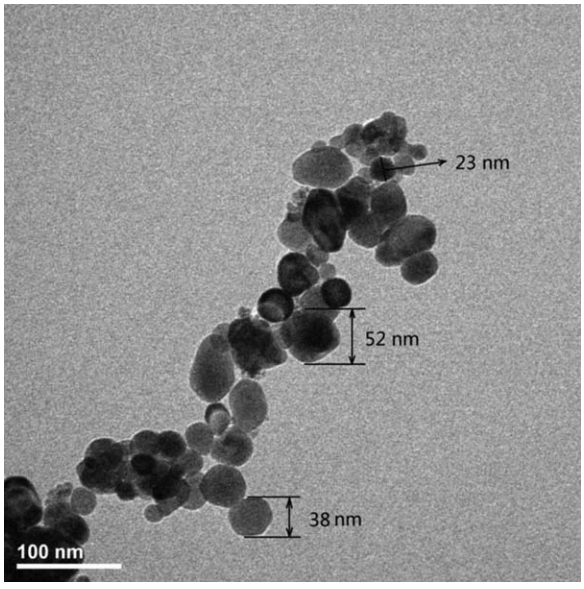

Figure 12. TEM image of N-CeO_2.

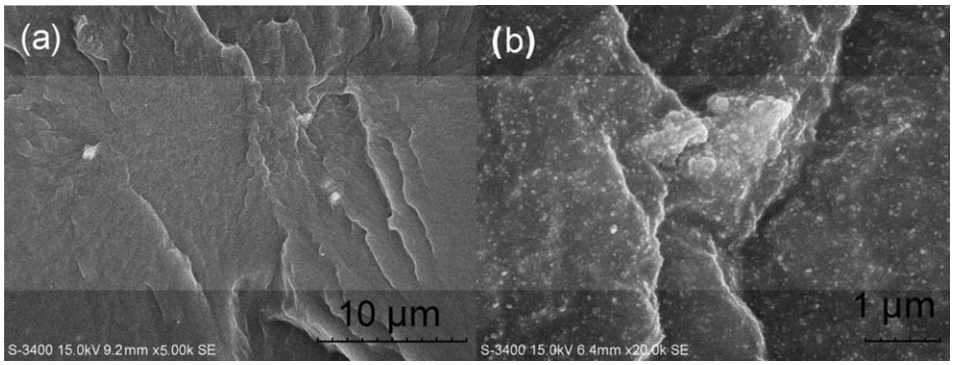

Figure 13. SEM images of fracture sections of PTFPMS/silica/mN-CeO_2 (100/40/2) with the magnifying power of (a) 5000 and (b) 20,000.

addition of mN-CeO_2 significantly improved the thermal stability of FSR. When mN-CeO_2 was added to the compound with an addition of 0, 1, 3, and 4 wt %, t90 (the time corresponding to 90% of initial weight) was 92, 156, 223, and 441 min, respectively. Besides, the residual weight has increased ~10% when the addition amount of mN-CeO_2 was varied from 0 to 4 wt %. In conclusion, ceria effectively inhibits the oxidation of FSR.

The Antioxidant Property of LS-CeO_2

Figure 5 shows the SEM images of MS-CeO_2 and LS-CeO_2. Compared with the ceria as sold in the market, the LS-CeO_2, which was prepared by precipitation process revealed lamellar structures with about 100 nm in thickness. Such lamellar structure has larger specific surface area than the rod-like structure. However, LS-CeO_2 revealed bad dispersibility when using as additive for FSR. The SEM image of fracture sections of PTFPMS/silica/LS-CeO_2 compound [see Figure 6(a)] exhibited serious aggregation of LS-CeO_2.

To prevent the aggregation of ceria, the surface of LS-CeO_2 was modified with silane coupling agent KH570. Figure 7 shows the surface modification mechanism.[33,34] There were plenty of hydroxyl groups on the surface of CeO_2 particles. After the hydrolysis of Si—OCH_3, the resulting silanol groups would dehydrate with hydroxyl groups of CeO_2 particles. In the end of this process, the surface of CeO_2 particle was covered by hydrophobic organics.

Figure 8 shows the X-ray diffraction patterns of MS-CeO_2, LS-CeO_2, and mLS-CeO_2. As seen from this figure, XRD patterns of the three ceria samples are similar. The characteristic peaks located at $2\theta = 28.51$, 32.96, 47.41, 56.23, and 58.93° corresponding to (111), (200), (220), (311), and (222) planes, respectively. The patterns are very close to the ones with cubic fluorite structured CeO_2 crystal in JCPDS database. The surface modification has also not changed the cubic fluorite structure.

Figure 9 demonstrates the TS of PTFPMS/silica, PTFPMS/silica/MS-CeO_2, PTFPMS/silica/LS-CeO_2, and PTFPMS/silica/mLS-CeO_2 before and after aging at 230 °C for 70 h. From the data of the initial TS (before aging), sample of PTFPMS/silica had the best strength at ~8.5 MPa, while compounds incorporating of ceria revealed different degrees of decrease. The TS of PTFPMS/silica/mLS-CeO_2 was 1–2 MPa higher than that of PTFPMS/silica/LS-CeO_2, indicating the former has a better dispersibility of CeO_2 in the compound than the latter one. The addition of MS-CeO_2 has significantly decreased the TS, because of the large scale and the bad dispersibility in the compound.

From the change rate of ΔTS after thermal aging, the addition of 2 wt % of mLS-CeO_2 showed only −9% of change rate after aging, while the compound without ceria has −58% of change rate after aging. Therefore, the addition of mLS-CeO_2 revealed a significant improvement on the thermal stability of FSR composites.

The FSR incorporating of LS-CeO_2 also showed an improvement on the thermal stability, between samples comprised of MS-CeO_2 and mLS-CeO_2. ΔTS basically decreased with the increasing addition of LS-CeO_2.

Figure 10 shows the elongation at break of PTFPMS/silica, PTFPMS/silica/MS-CeO_2, PTFPMS/silica/LS-CeO_2 and PTFPMS/

Table II. The Mechanical Properties and Change Rate for FSR after Thermal Oxidative Aging for 70 h at 250 °C

Composition	PTFPMS/silica	PTFPMS/silica/mLS-CeO_2	PTFPMS/silica/mN-CeO_2			
Addition of ceria (wt %)	0	2	0.5	1	2	3
Hardness (Shao A)	70	68	71	70	72	70
TS (MPa)	7.5	7.4	7.5	7.3	7.3	7.4
Elongation at break (%)	281	273	252	280	280	265
250°C × 70 h ageing						
Hardness change (Shao A)	+27	+11	+9	+10	+8	+9
TS change (%)	—	−58.4	−44	−38.4	−27.4	−28.8
Elongation at break change (%)	—	−51.8	−52.4	−50	−36.1	−34.9

silica/mLS-CeO_2 before and after aging at 230 °C for 70 h. The results are consistent with those of TS. The FSR incorporating of PTFPMS/silica/mLS-CeO_2 has the best thermal stability. The change rate of elongation at break (ΔE) is −15% after aging for 70 h at 230 °C.

In general, the thermal stability improvement of FSR, which could be reflected by ΔTS or ΔE, is determined by the contact area between ceria and FSR (A_c), where A_c is influenced by the specific surface area of ceria (A_s), the addition amount of ceria (W) and the degree of dispersion (α). The relationship could be expressed in eq. (2) as follows:

$$A_c \propto A_s W \alpha \tag{2}$$

where the scope of α is from 0 to 1, where $\alpha = 1$ represents that the ceria particles are individually and uniformly distributed inside the FSR.

For FSR incorporating of 2 wt % of ceria, A_s(MS-CeO_2) < A_s(LS-CeO_2) = A_s(mLS-CeO_2), and α(MS-CeO_2) = α(LS-CeO_2) < α(mLS-CeO_2). As a result, A_c(MS-CeO_2) < A_c(LS-CeO_2) < A_c(mLS-CeO_2). The FSR incorporating of mLS-CeO_2 has the largest contact area, and therefore reveals the best thermal stability.

The Antioxidant Property of N-CeO_2

To obtain ceria with larger specific surface area, ceria nanoparticles were prepared by SCS, following the reaction scheme shown below:

$$Ce(NO_3)_3\,6H_2O + \varphi HOCH_2 + \frac{1}{2}O_2 \rightarrow CeO_2 + \frac{3}{2}N_2 + 2\varphi CO_2 + (6+3\varphi)H_2O$$

Figure 11 shows the XRD patterns of N-CeO_2 when φ equals to 0.75, 1, 1.5, and 2.25. The characteristic peaks located at $2\theta = 28.55$, 32.98, 47.39, 56.27, and 58.93° corresponding to (111), (200), (220), (311), and (222) planes, respectively. By Scherrer equation, the crystallite size of N-CeO_2, d_{XRD}, were calculated as 7.65, 15.3, 16.8, and 18.7 nm, respectively.

Figure 12 shows the TEM image of N-CeO_2 when $\varphi = 0.75$. The N-CeO_2 had a nano-sized spherical structure with 20–50 nm in diameter. It possessed much larger specific surface area than MS-CeO_2 and LS-CeO_2.

Figure 13 shows the SEM images of fracture sections of PTFPMS/silica/mN-CeO_2 (100/40/2). The mN-CeO_2 revealed a homogeneous distribution in the FSR compounds.

The FSR incorporating of mLS-CeO_2 and mN-CeO_2 were, respectively, performed thermal aging tests at 250 °C for 70 h and the results are shown in Table II. After aging, the FSR without ceria became quite brittle and the elasticity was lost entirely. However, the FSR incorporating of mLS-CeO_2 and mN-CeO_2 revealed a definite retention rate of mechanical properties. Compared with thermal aging results for 230 °C × 70 h, the PTFPMS/silica/mLS-CeO_2 showed a significant increase on ΔTS (from −9 to −58.4%) and ΔE (from −15 to −51.8%), indicating that mLS-CeO_2 might not be suitable to be used at 250 °C.

The FSR containing 2 wt % of modified N-CeO_2 maintained 72.6% of TS (ΔTS = −27.8%) and 63.9% of elongation at break (ΔE = −31.6), respectively, while FSR without ceria completely failed. The results showed that the FSR, when incorporating of mN-CeO_2, revealed a significant improvement on the thermal stability. Since the mN-CeO_2 has the largest A_s and α is close to 1, the A_c is thus the largest one among all samples and therefore has the best thermal stability according to eq. (2).

CONCLUSIONS

The focus of this study was to improve the heat resistance of FSR. Firstly, the study of degradation mechanism of PTFPMS (or FSR) indicated, at temperatures below 350 °C, degradation resulted from the oxidation scission of the side groups played a more important role than that resulted from the siloxane rearrangement. Secondly, the addition of ceria had significantly improved the thermal stability of FSR by inhibiting the oxidation scission. Furthermore, the surface modified laminar-structure ceria and nanoparticle ceria, which had larger specific surface area and good dispersibility, presented significant antioxidant effect at 230 and 250 °C, respectively. The findings from this work were of importance in guiding the preparation of FSR with high temperature resistance for various industry applications.

ACKNOWLEDGMENTS

The research was supported by Shanghai Leading Academic Discipline Project (B502) and Shanghai Key Laboratory Project (08DZ2230500). The authors gratefully acknowledge the financial support of the National Science Foundation of China (Grant 51573043) and the Fundamental Research Funds for the Central Universities (No. 2015ZD25). Support from FSIR Advanced Material Co., Ltd. is also gratefully acknowledged.

REFERENCES

1. Xu, C.; Wang, Y.; Lin, B.; Liang, X.; Chen, Y. *Mater. Des.* **2015**, *88*, 170.
2. Nie, F.; He, G.; Zhao, W.; Ju, J.; Liu, Y.; Dai, Y. *J. Polym. Res.* **2014**, *21*, 319.
3. Xu, T.; Liu, H.; Song, J.; Shang, S.; Song, Z.; Zou, K.; Yang, C. *J. Polym. Sci. Part A: Polym. Chem.* **2015**, *53*, 1769.
4. Liu, Y.; Liu, H.; Zhang, R.; Zhou, C.; Feng, S. *Polym. Eng. Sci.* **2013**, *53*, 52.
5. Dai, Y.; Ruan, X.; Bai, F.; Yu, M.; Li, H.; Zhao, Z.; He, G. *Appl. Surf. Sci.* **2016**, *360*, 164.
6. Cypryk, M.; Delczyk, B.; Juhari, A.; Koynov, K. *J. Polym. Sci. Part A: Polym. Chem.* **2009**, *47*, 1204.
7. Drobny, J. G. *Polym. Adv. Technol.* **2007**, *18*, 117.
8. Xu, X.; Xu, Z.; Chen, P.; Zhou, X.; Zheng, A.; Guan, Y. *J. Inorg. Organomet. Polym.* **2015**, *25*, 1267.
9. Esmizadeh, E.; Naderi, G.; Barmar, M. *Fiber Polym.* **2014**, *15*, 2376.
10. Lin, C. W.; Chien, C. H.; Tan, J.; Chao, Y. J.; Van Zee, J. W. *J. Power Sources* **2011**, *196*, 1955.
11. Rizzo, J.; Harris, F. W. *Polymer* **2000**, *41*, 5125.

12. Bhuvaneswari, C. M.; Dhanasekaran, R.; Chakravarthy, S. K. R.; Kale, S. S.; Gouda, G. *Prog. Rubber Plast. Re* **2015**, *31*, 207.
13. Longuet, C.; Ratsimihety, A.; André, S.; Boutevin, G.; Guida-Pietrasanta, F.; Decamps, B.; Ramonda, M.; Joly-Duhamel, C.; Ganachaud, F. *J. Mater. Chem.* **2010**, *20*, 10269.
14. Su, Z. T. *J. Appl. Polym. Sci.* **1999**, *73*, 2779.
15. Yang, Z.; Han, S.; Zhang, R.; Feng, S.; Zhang, C.; Zhang, S. *Polym. Degrad. Stab.* **2011**, *96*, 2145.
16. Kählig, H.; Zöllner, P.; Mayer-Helmc, B. X. *Polym. Degrad. Stab.* **2009**, *94*, 1254.
17. Bernstein, R.; Gillen, K. T. *Polym. Degrad. Stab.* **2009**, *94*, 2107.
18. Cornelius, D. J.; Monroe, C. M. *Polym. Eng. Sci.* **1985**, *25*, 467.
19. Sim, L. C.; Ramanan, S. R.; Ismail, H.; Seetharamu, K. N.; Goh, T. *J. Thermochim. Acta* **2005**, *430*, 155.
20. Min, C. Y.; Huang, Y. D.; Liu, L. *J. Mater. Sci.* **2007**, *42*, 8695.
21. Li, Y.; Zheng, Z.; Xu, C.; Ren, C.; Zhang, Z.; Xie, Z. *J. Appl. Polym. Sci.* **2003**, *90*, 306.
22. Han, W. Q.; Wu, L.; Zhu, Y. *J. Am. Chem. Soc.* **2005**, *127*, 12814.
23. Wang, Z.; Feng, X. *J. Phys. Chem. B* **2003**, *107*, 13563.
24. Chen, W.; Li, F.; Yu, J. *Mater. Lett.* **2007**, *61*, 397.
25. Chen, W.; Li, F.; Yu, J. *Mater. Lett.* **2006**, *60*, 57.
26. Radhakrishnan, T. S. *J. Appl. Polym. Sci.* **1999**, *73*, 441.
27. Grassie, N.; Macfarlane, I. G. *Polym. Eng. Sci.* **2010**, 2440.
28. Gao, Y.; Jiang, W.; Guan, Y.; Yang, P.; Zheng, A. *Polym. Eng. Sci.* **2010**, 2440.
29. Li, Z. X.; Li, L. L.; Yuan, Q.; Feng, W.; Xu, J.; Sun, L. D.; Song, W. G.; Yan, C. H. *J. Phys. Chem. C* **2008**, *112*, 18405.
30. Xue, Y.; Luan, Q.; Yang, D.; Yao, X.; Zhou, K. *J. Phys. Chem. C* **2011**, *115*, 4433.
31. Korsvik, C.; Patil, S.; Seal, S.; Self, W. T. *Chem. Commun.* **2007**, *10*, 1056.
32. Chinn, S.; De Teresa, S.; Sawvel, A.; Shields, A.; Balazs, B.; Maxwell, R. S. *Polym. Degrad. Stab.* **2006**, *91*, 555.
33. Deetz, J. D.; Faller, R. *J. Phys. Chem. B* **2014**, *118*, 10966.
34. Suzuki, N.; Yatsuyanagi, F.; Ito, M.; Kaidou, H. *J. Appl. Polym. Sci.* **2002**, *86*, 1622.